Numerical evaluation of an optically switchable photovoltaic glazing system for passive daylighting control and energy-efficient building design

Xiao Liu , Yupeng Wu [*]

Department of Architecture and Built Environment, Faculty of Engineering, The University of Nottingham, University Park, Nottingham, NG7 2RD, United Kingdom

ABSTRACT

Adaptive control of solar heat gain and visible light transmission through windows is perceived to be a potential measure for enhancing energy conservation and visual comfort in buildings. In this study, a novel versatile window, named Building Integrated Photovoltaic (BIPV) smart window, was proposed to offer simultaneous improvement of daylighting control, on-site electricity generation and building energy efficiency, compared to traditional BIPV windows with static optical properties. The key components of the proposed system include an optically switchable thermotropic layer made of Hydroxypropyl Cellulose (HPC) hydrogel, crystalline-silicon photovoltaic cells, clear glass and low-emissivity (low-e) glass covers. The thermotropic layer can respond to heat by autonomously changing its visible and near-infrared optical properties, with which the amount of solar radiation into building spaces can be manipulated and thus the risks of excessive solar heating and illumination can be prevented. Apart from excellent solar modulation, the BIPV smart window can collect a proportion of the light scattered from the thermotropic layer and concentrate it onto the integrated PV cells for extra electricity generation. An innovative methodology has been proposed to predict the optical, thermal and electrical properties of the BIPV smart window under varying ambient conditions. Numerical simulations have been carried out in EnergyPlus to predict the window's performance when it is applied to an office-type environment in the climate of Nottingham, the UK. The influence of different window design scenarios, in terms of Window-to-Wall Ratio (WWR), orientation and transition temperature, has been investigated. It was found that using the BIPV smart window can achieve an annual energy saving of 36.6% but also a more comfortable indoor luminous environment, compared to the counterpart BIPV window (with no thermotropic layer integrated), when installed in the south-oriented office with a WWR of 25%.

1. Introduction

Maximising the utilisation of the solar energy incident on building envelopes has been identified as an important strategy in sustainable building design [1]. Increasing the ratio of transparent and opaque surface areas in a building envelope can promote passive solar heating and lighting in the indoor environment. However, there are multiple challenges faced by building envelopes with large glazing areas, such as excessive daylighting, heat gain and heat loss, which may increase the risks of thermal and visual discomfort of occupants and also the energy demands for space cooling and heating [2]. These difficulties can be mitigated by applying glazing systems with improved performance in terms of thermal insulation (e.g., vacuum glazing [3]), solar control (e. g., smart glazing [4]) or both (e.g., evacuated smart glazing [5] and Parallel Slats Transparent Insulation Material (PS-TIM) glazing [6]).

Choosing an appropriate glazing system for a building geometry under a specific climatic condition is a crucial step in the design of passive solar buildings. This creates a strong need for researchers to investigate the combined effect of various glazing design parameters such as glazing properties, Window-to-Wall Ratio (WWR), inclination and orientation on building energy efficiency and indoor thermal and luminous environments [2].

The performance of glazing systems can be measured in real buildings or through full/reduced-scale outdoor test facilities [7] or predicted using building performance simulation software (e.g., EnergyPlus, ESP-r, TRANSYS) and daylight analysis software (e.g., RADIANCE) [8, 9]. Field tests in real buildings can give the most lifelike outcomes [7]. However, it is difficult to reproduce the tests and control the test conditions such as occupants' behaviour. What is more, data obtained for buildings under different climatic conditions can hardly be compared

---

because of the peculiar architectural and operating features of each building [7]. Numerical simulation tools offer the advantages of being replicable and allowing users to compare glazing performance under different climatic conditions and identify optimal design strategies by adjusting input parameters to models. Nevertheless, with innovations and advancements in glazing technology, continuous efforts are required to incorporate new algorithms and capabilities in the simulation tools or couple them with other programs such as Computational Fluid Dynamics (CFD) [6,8] and ray tracing [10] to yield accurate results.

There is an extensive body of research on the performance of advanced glazing technologies, comprising numerical and experimental investigations. Thermochromic (TC) glazing is a type of smart glazing technologies, which can regulate the amount of solar heat and light into a building space by changing its colour and transparency autonomously under varying ambient temperatures. Hoffmann et al. [11] investigated the energy-saving potential of a hypothetical TC window when installed in a prototypical office building under the mixed hot/cold climatic condition of Chicago (the US). EnergyPlus simulations were conducted for the TC window in different design scenarios (e.g., WWRs, orientations and transition temperature ranges), showing a maximum annual energy saving of 14% in comparison with a commercially available low-emissivity (low-e) glazing. Warwick et al. [12] modelled a vanadium dioxide (VO_2) based TC window in a cellular office room in a variety of climates. The results obtained for the climate of London (the UK) suggested that the TC window with the lowest transition temperature (20 °C) and the sharpest transition gradient (25% transmittance change per 1 °C) can afford the largest reduction in annual total energy demand, approximately 47% compared to an ordinary double-glazed window. Liang et al. [13] performed a comparative analysis of three different types of TC glazings: double-glazed units containing a VO_2 nanoparticle film, a composite film of ionic liquid containing $[bmim]_2$ $NiCl_4$ and a combination of both films. EnergyPlus simulations were carried out based on a typical cellular office room tested in different climatic regions of China. It was found that the TC glazing with a larger difference in near-infrared (NIR) light transmittance (between its clear and tinted states) can yield a more significant energy saving, while that with a larger modulation of visible light transmittance can achieve a more comfortable indoor luminous environment. Aburas et al. [14] compared the performance of TC glazings based on VO_2 nanoparticles with different coating thicknesses (between 80 and 800 nm) by experimental characterisations, followed by EnergyPlus simulations. The results revealed that with a thicker coating, the TC glazing can provide a larger transmittance modulation in the NIR region, thus contributing to a larger annual energy saving, for example, from 9.91% (80 nm) to 33.31% (800 nm) in the climate of London, which confirms the findings of Liang et al. [13]. A review paper on existing simulation methods for TC windows has been published by Aburas et al. [15].

Thermotropic (TT) glazing is another type of passive smart glazing technologies. In contrast to TC glazing, TT glazing features a transparent-scattering switching behaviour in response to heat, i.e., below the transition temperature, TT glazing behaves as a clear glazing with high solar and visible light transmittance; above the transition temperature, it switches to a light-scattering state with reduced transmittance, which can protect the adjacent room space from excessive solar heating and daylighting. Li et al. [16] developed a TT smart window based on poly(N-isopropylacrylamide) (PNIPAm) and 2-aminoethylmethacrylate hydrochloride (AEMA) co-polymerized hydrogel micro-particles. The smart window has a transition temperature of 32 °C and transmission modulations of 87% in the visible range (380–780 nm), 76% in the near-infrared range (780–2500 nm) and 81% over the solar spectrum (250–2500 nm). Wu and his research team [17–19] introduced a thermotropic hydrogel consisting of Hydroxypropyl Cellulose (HPC) and gellan gum for smart window applications [19]. A simulation case study was conducted under the hot summer Mediterranean climatic condition of Palermo (Italy) and demonstrated

that the 6 wt % HPC based TT window with a transition temperature range of 35–45 °C can offer an annual energy saving of 23%, compared to an equivalent double-glazed unit. The energy-saving potentials of smart windows based on thermotropic materials such as PNIPAm and Hydroxypropyl Methylcellulose (HPMC) have been reported in the literature [20,21].

In recent years, a new class of advanced windows combing TT glazing and photovoltaic (PV) cells has emerged, aiming to improve the daylighting control and electricity generation performance of traditional Building Integrated PV (BIPV) windows [17,18,22]. By adding a thermotropic layer to a double or triple glazed BIPV window, the amount of daylight reaching the interior of buildings can be adaptively controlled, i.e., the window solar heat gain and visible transmittance are reduced as the BIPV window is subjected to a higher ambient temperature or more intense solar irradiation. In the meantime, the electric power outputs of the window integrated photovoltaic cells are improved, due to the solar concentration effect which is induced by the light scattering (from the TT layer) and the Total Internal Reflection (TIR) effect [17,18]. The concept has been proved by previous studies through ray-tracing simulation [17,23,24], indoor experiment [24] and outdoor experiment [25]. Nevertheless, there is a lack of knowledge concerning the behaviour of such systems in the context of buildings and their influence on building energy consumption, indoor luminous environment, and occupant comfort.

In this study, a novel BIPV smart window system which consists of a combined photovoltaic thermotropic glazing cover (named 'glass-PV-TT-glass laminate'), an air gap and a low-e glazing cover has been designed and numerically evaluated. This study aims to provide a facile and reliable approach to model the dynamic optical/thermal/electrical properties of the proposed system and couple these window properties to a Building Performance Simulation (BPS) model to predict its effects on building energy performance and visual comfort. The BPS model has been developed using EnergyPlus and the simulation has been conducted for a cellular office room with the proposed system under the climatic condition of Nottingham (the UK). Parametric analysis to aid in the window design and optimisation has been performed with respect to various WWRs (25%, 50% and 75%), glazing orientations (south, west, east and top) and TT transition temperatures (between 20 °C and 40 °C).

2. Methodology

This paper presents a comprehensive approach to modelling and optimal design of the proposed BIPV smart window system. Numerical methods for obtaining the system's optical, thermal and electrical properties have been developed and validated. An EnergyPlus model incorporating these properties has been developed to explore the potentials of the BIPV smart window system in reducing the overall energy consumption and the occurrence of excessive levels of solar heat gain and daylight within an office-type environment, as compared with the cases of applying conventional windows.

2.1. Overview of the simulation method

EnergyPlus, a whole building energy simulation program, has been widely used to evaluate the thermal and energy performance of PV windows [26–29] and PV Double-Skin Façades (PV-DSFs) [30,31]. Compared with previous research using fixed optical properties to define semi-transparent BIPVs in EnergyPlus, modelling the proposed BIPV smart window system can be more challenging because its optical properties such as visible/solar transmittance, reflectance, absorptance and angular scattering distribution are dynamic. These variables depend on the temperature of the thermotropic layer of the system that is influenced by its surrounding environment and varies over time. Moreover, such variation affects the electricity generation rate of the integrated PV cells, because the amount of solar energy being concentrated onto and absorbed by the PV cells is related to the scattering
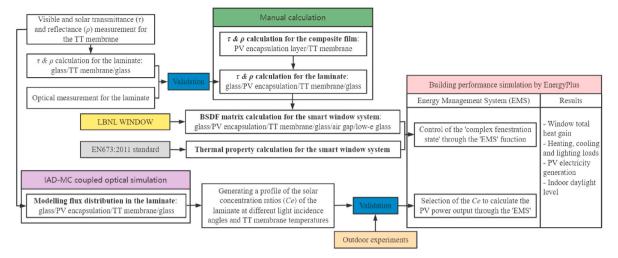
Fig. 1. Flow chart illustrating the model development process for the BIPV smart window system.

properties as well as spectral properties of the thermotropic layer. Although EnergyPlus has built-in modules for PV panel ('Generator: Photovoltaic') and thermochromic glazing (i.e., 'Window-MaterialGlazingGroup:WindowMaterialGlazingGroup: Thermochromic'), these modules are overly simple and inadequate when it comes to modelling a complex fenestration that encompasses Concentrating PV (CPV), thermochromism and light scattering features. Therefore, a method able to reliably predict the dynamic behaviour of the proposed system needs to be developed.

The workflow in Fig. 1 shows the process of predicting the optical, thermal and electrical properties of the proposed system and then coupling these properties to an EnergyPlus model for building performance simulation. Details of the calculation/simulation methods are described in **Sections 2.2-2.4**.

2.1.1. Optical property calculation method

The optical property calculation was carried out in two main steps: (1) obtaining the spectral transmittance (τ) and reflectance (ρ) of the laminate which is made up of a front glass, PV encapsulation layer, TT membrane layer and rear glass; (2) obtaining the Bi-directional Scattering Distribution Function (BSDF) data (i.e., angularly resolved transmission and reflection data) of the smart window system which consists of the above laminate, an air gap and rear glass. The window configuration is presented in **Section 2.2**. For the first step, a net

radiation method proposed by Laouadi and Parekh (2007) [32] was adopted to manually calculate the laminate's properties. Prior to the calculation, the net radiation method was validated by comparing the optical properties calculated and measured for a sample of TT laminated glazing which was comprised of a TT membrane layer between two pieces of glass. For the second step, the spectral properties of the glass-PV-TT-glass laminate were input to the software LBNL WINDOW where Klems' matrix multiplication algorithm was implemented to generate BSDF datasets for the smart window system (i.e., 145 × 145 matrices at different wavelengths, each of which corresponds to 145 incident light directions and 145 outgoing directions of light transmitted or reflected on the window surface) [10,33]. Alternatively, the system's BSDFs can be calculated using genBSDF, a ray-tracing program embodied within RADIANCE [10,34,35].

2.1.2. Thermal property calculation method

The thermal properties of the BIPV smart window system such as thermal transmittance (U-value) were calculated according to the European Standard EN 673:2011 [36]. The system's thermal properties along with the BSDF datasets were encoded and transformed into EnergyPlus compatible files through LBNL WINDOW.

2.1.3. Electrical property calculation method

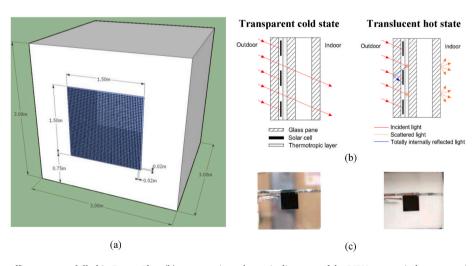A PV power calculation algorithm was developed to predict the

Fig. 2. (a) Geometry of the office room modelled in EnergyPlus, (b) cross-section schematic diagrams of the BIPV smart window system in different states, (c) photos of the glass-PV-TT-glass laminate in different states.

Table 1
Window components and their thicknesses.

Type	Outer cover	Middle layer	Inner cover
BIPV smart window	**Laminate** (from outside to inside): 3 mm GPE scientific optiwhite glass[a] 2 mm PV encapsulation layer[b] 1 mm thermotropic hydrogel layer 3 mm GPE scientific optiwhite glass	12 mm air gap	3 mm low-e glass (ClimaGuard 80/70)[c]
Counterpart BIPV window	**Laminate** (from outside to inside): 3 mm GPE scientific optiwhite glass 2 mm PV encapsulation layer 3 mm GPE scientific optiwhite glass	12 mm air gap	3 mm low-e glass
Low-e double glazing	6 mm GPE scientific optiwhite glass	12 mm air gap	3 mm low-e glass

[a] A low-iron optical glass with a refractive index of 1.51 at the wavelength of 600 nm.

[b] Talsun c-Si PV cells embedded in a Dow-Corning 1–2577® coating with a refractive index of 1.49 (@600 nm).

[c] A low-e glass with emissivities of 0.1 facing the air gap and 0.84 facing the indoors [38].

electrical performance of the glass-PV-TT-glass laminate. The algorithm is based on a profile of solar concentration ratio against TT layer temperature and solar incidence angle, which was derived by using the Inverse-Adding-Doubling and Monte-Carlo (IAD-MC) coupled optical model reported in our previous study [23]. The algorithm was validated by the outdoor experimental results from our previous study [25] and subsequently applied in EnergyPlus to predict the on-site electricity generation by the BIPV smart window system in buildings.

2.1.4. Building performance simulation (BPS) method

To achieve the adaptive changes of the optical and electrical properties of the BIPV smart window system in response to varying weather conditions, a built-in function of EnergyPlus called 'Energy Management System (EMS)' was implemented. In brevity, the EMS sensed parameters such as window surface temperature and solar incidence angle, and accordingly changed the window state by (1) overriding the 'complex fenestration construction' with updated BSDF properties and (2) re-selecting the solar concentration ratio for PV power calculation. Through the building performance simulations, the proposed system can be evaluated from multiple perspectives such as energy saving and control of solar heat gain and daylighting, and can be optimised in terms of WWR, orientation and optical switching temperature.

2.2. BPS model geometry and window configuration

The BPS model was based on a cellular office room with dimensions of 3 m × 3 m × 3 m, as shown in Fig. 2(a). The office room was considered as a south-facing perimeter zone of an office building and buffered by mechanically conditioned spaces. It was assumed that only the south wall and horizontal roof of the office room were exposed to the outdoor environment and subjected to heat transfer [19,37]. The office room had a BIPV smart window with dimensions of 1.5 m × 1.5 m on its south wall, equivalent to a WWR of 25%. The window consisted of a glass-PV-TT-glass laminate (outer cover), an air gap and a low-e glass pane (inner cover), as presented in Table 1 and Fig. 2(b). Inside the glass-PV-TT-glass laminate was an array of crystalline-silicon (c-Si) PV cells with cell dimensions of 0.01 m × 0.01 m, a cell-to-cell spacing of 0.02 m and a PV coverage ratio of 11% (i.e., the fraction of the window aperture surface area covered by the PV cells). The PV cells were encapsulated in a dielectric coating layer, which enabled the PV cells to be optically bonded to the front glass cover but also electrically isolated from the back thermotropic hydrogel layer.

In principle, during cold periods, the BIPV smart window system allows the penetration of solar radiation into the building space, while during hot periods, it scatters the incident solar radiation and provides solar shading for the interiors, as sketched in Fig. 2(b). As a consequence, the quantities of solar heat and visible light into the building space can be adaptively controlled. Meanwhile, a proportion of the scattered light is collected by the PV cells (due to total internal reflection) and converted into electricity. Therefore, the electric power output of the BIPV window can be potentially improved when the TT hydrogel layer switches from transparent to light-scattering. Fig. 2(c) shows the transition of the glass-PV-TT-glass laminate from a transparent state to a translucent state when increasing the TT layer temperature from 25 °C to 40 °C. A detailed description of the thermotropic hydrogel layer is given in Section 2.3.1.

For a comparative analysis, simulations were conducted for the three cases where the office room was installed with (1) the proposed BIPV smart window, (2) a conventional BIPV window (with no thermotropic layer), (3) a low-e double-glazed window (with no thermotropic layer and PV cells). The window configurations are detailed in Table 1.

2.3. Calculation of the window's dynamic properties

For the sake of developing an accurate BPS model, the input parameters including the dynamic properties of the BIPV smart window system need to be accurately defined. This section describes the methods to obtain the dynamic properties of the BIPV smart window system through optical measurement (Section 2.3.1), optical calculation (Section 2.3.2), thermal calculation (Section 2.3.3) and electrical calculation (Section 2.3.4).

2.3.1. Optical properties of the thermotropic hydrogel membrane

The thermotropic hydrogel reported in our previous study [25] was selected for the smart window development. The TT hydrogel membrane was synthesised of 6 wt % hydroxypropyl cellulose (HPC), 4.5 wt
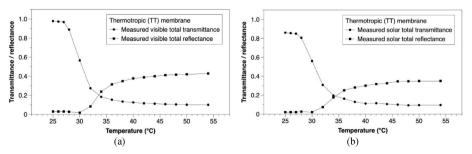

Fig. 3. Average optical properties of the TT membrane of 1 mm thickness at different membrane temperatures (a) in the visible region (380–780 nm) and (b) over the solar spectrum (300–2500 nm). The spectral transmittance and reflectance of the laminate were measured by using the spectrometers Ocean Optics USB2000+VIS-NIR-ES (300–1000 nm) and NIRQuest 512–2.5 (1000–2500 nm) equipped with the integrating spheres Ocean Optics FOIS-1 (for transmission tests) and ISP-REF (for reflection tests).
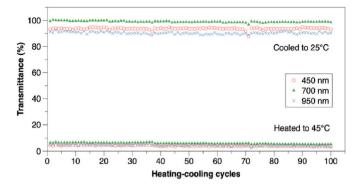
Fig. 4. Spectral transmittance of the 6 wt % HPC, 0.5 wt % GGF, 4.5 wt % NaCl based hydrogel membrane at 3 mm thickness over 100 heating-cooling cycles. The cycling test was conducted using the USB2000+VIS-NIR-ES spectrometer and the Qpod-2e temperature-controlled sample compartment.

% sodium chloride (NaCl) and 0.5 wt % gelling agent. Its average transmittance and reflectance in the visible region (300–1000 nm) and over the solar spectrum (300–2500 nm) at different membrane temperatures were measured by using spectrometers with integrating spheres. As can be seen from Fig. 3 (a) and (b), the TT hydrogel membrane at 1 mm thickness had high visible transmittance (>90%) and solar transmittance (>80%) at room temperature, which started to decline at 28 °C and halved at 30.5 °C (i.e., the transition temperature) and reduced to approximately 10% at 40 °C. Conversely, the visible and solar reflectance increased with the increasing membrane temperature. Fig. 4 shows that the hydrogel material had good thermal stability after repeated heating and cooling cycles between 25 °C and 45 °C. The measured optical properties of the TT hydrogel membrane are prerequisites to the optical calculation in Section 2.3.2 and the electrical calculation in Section 2.3.4.

2.3.2. Optical properties of the BIPV smart window

For a window system consisting of two clear glass panes separated by a non-absorbing air gap, the system's transmittance and reflectance can be calculated according to the International Standard ISO 9030:2003 [39]. However, if the window system has a non-specular glass pane or an internal shading device (e.g., Venetian blind), the simple calculation method may not be reliable, particularly for daylight analysis where the detail of outgoing light distribution is of significance. An alternative method is to use Bidirectional Scattering Distribution Functions (BSDF) to represent the angularly resolved transmission and reflection properties of a Complex Fenestration System (CFS) [40]. The BSDF approach has been widely used in research on CFS such as windows integrated with PVs [41], prismatic films [42], Parallel Slat Transparent Insulation Material (PS-TIM) structures [43] and thermotropic material based PS-TIM structures [35].

In this study, the proposed smart window system is composed of a low-e clear glass and a glass-PV-TT-glass laminate, the latter of which works as a specular glazing when the TT layer temperature is below 28 °C but converts to a scattering glazing when above 28 °C. Therefore, the BSDF approach was applied to predict the optical characteristics of the system in both clear and light-scattering states. To calculate the BSDF data, the optical properties of the glass-PV-TT-glass laminate such as the specular and diffuse transmittance and reflectance need to be known. These optical properties can be obtained by using integrating spheres with light traps to exclude or include the specular components of light transmission and reflection [10,40]. Laouadi and Parekh [32] proposed an optical model to predict the optical characteristics of a stack configuration of clear glass substrate(s) with an applied or laminated scattering film, and implemented the model in the SkyVision software tool. The advantages of this model are that it does not need a sophisticated computer program (e.g., ray tracing) and can be applied to thick laminates that are prone to measurement errors when using integrating spheres. On the other hand, the optical model was developed based on a net radiation method and assumed the light scattered off an object as

Fig. 5. Schematic diagrams illustrating the calculation procedures: (1) calculating the optical properties of the composite film (see the middle diagram) using the optical properties of the optical coating and TT membrane layers (see the right diagram) as input, based on the equations in Appendix A; (2) calculating the optical properties of the laminate (see the left diagram) using the optical properties of the composite film as input, based on the equations in Appendix B.
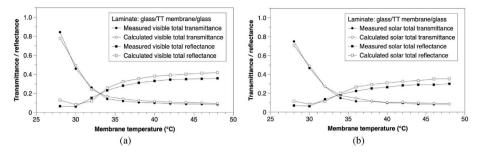
Fig. 6. Comparison between the calculation and integrating-sphere measurement for the (a) visible and (b) solar optical properties of a glazing sample that consisted of a TT membrane (1 mm thick) between two pieces of GPE optical glass (3 mm thick).

Table 2
Visible and solar optical properties of the glass-PV-TT-glass laminate derived from manual calculation.

		Front beam-to-specular transmitt-ance	Front beam-to-diffuse transmitt-ance	Front beam-to-specular reflectan-ce	Front beam-to-diffuse reflectan-ce	Back beam-to-specular transmitt-ance	Back beam-to-diffuse transmitt-ance	Back beam-to-specular reflectan-ce	Back beam-to-diffuse reflectan-ce
		$\tau_{f,bs,l}$	$\tau_{f,bd,l}$	$\rho_{f,bs,l}$	$\rho_{f,bd,l}$	$\tau_{b,bs,l}$	$\tau_{b,bd,l}$	$\rho_{b,bs,l}$	$\rho_{b,bd,l}$
Visible	26 °C	0.775	0	0.123	0	0.775	0	0.123	0
	28 °C	0	0.673	0.073	0.063	0	0.635	0.041	0.120
	30 °C	0	0.425	0.073	0.030	0	0.401	0.041	0.054
	36 °C	0	0.124	0.073	0.222	0	0.117	0.041	0.254
	48 °C	0	0.086	0.073	0.299	0	0.081	0.041	0.338
Solar	26 °C	0.681	0	0.110	0	0.681	0	0.103	0
	28 °C	0	0.609	0.073	0.054	0	0.574	0.041	0.102
	30 °C	0	0.422	0.073	0.031	0	0.398	0.041	0.055
	36 °C	0	0.129	0.073	0.176	0	0.121	0.041	0.203
	48 °C	0	0.075	0.073	0.247	0	0.071	0.041	0.280

isotropic diffuse, which however might not be accurate if the object shows narrow-angle scattering or multi-peak scattering in reality.

In this study, the optical properties of the glass-PV-TT-glass laminate were estimated using the optical model of Laouadi and Parekh with the equations [32] listed in **Appendices A and B**. The modelling approach is presented in Fig. 5. The laminate was divided into three layers: two clear glass substrates and a composite film, the latter of which is a combination of an optical coating, opaque PV cells and a TT membrane layer. In the first step, the optical properties of the composite film were calculated from **Equations (A1)-(A8)**, including the front beam-to-specular transmittance ($\tau_{f,bs,c}$) and reflectance ($\rho_{f,bs,c}$), front beam-to-diffuse transmittance ($\tau_{f,bd,c}$) and reflectance ($\rho_{f,bd,c}$), back beam-to-specular transmittance ($\tau_{b,bs,c}$) and reflectance ($\rho_{b,bs,c}$), back beam-to-diffuse transmittance ($\tau_{b,bd,c}$) and reflectance ($\rho_{b,bd,c}$). For simplicity, the diffuse-to-diffuse transmittances ($\tau_{f,d,c}$, $\tau_{b,d,c}$) and reflectances ($\rho_{f,d,c}$, $\rho_{b,d,c}$) of the composite film were assumed to be the same as its beam-to-diffuse properties. In the second step, the composite film's optical properties were inputted to **Equations (B1)-(B4)** to calculate the laminate's optical properties (labelled as $\tau_{x,x,l}$ and $\rho_{x,x,l}$ in Fig. 5). Details of the calculations are provided in **Appendices A and B**.

Prior to the calculations, a three-layer glazing sample consisting of a TT membrane laminated with low-iron optical glass slides was developed for validation of the optical model. The measured total transmittance and reflectance of the thermotropic membrane at different temperatures presented in Fig. 3 were inputted to **Equations (B1)-(B4)**. An assumption was made that in the scattering state (above 28 °C), all of the transmitted/reflected light was in the diffuse form (i.e., $\tau_{f,bs,c}$, $\tau_{b,bs,c}$, $\rho_{f,bs,c}$, $\rho_{b,bs,c} = 0$). Fig. 6 shows the calculated and measured results for the laminate's hemispherical transmittance and reflectance (i. e., the sum of the beam-to-specular and beam-to-diffuse properties). A reasonable agreement was observed with some discrepancies, probably due to the above ideal assumption or because the model calculates the flux balance at the interface between media using a single parameter reflectivity (r_s) without considering the critical angle and occurrence of total internal reflection.

The calculated visible and solar optical properties of the glass-PV-TT-glass laminate at different TT layer temperatures are given in Table 2. When heated from 26 °C to 28 °C, the laminate's beam-to-diffuse transmittance ($\tau_{f,bd,l}$, $\tau_{b,bd,l}$) increased while its beam-to-specular transmittance ($\tau_{f,bs,l}$, $\tau_{b,bs,l}$) reduced to 0%, indicating its transformation from a specular glazing to a diffusing glazing. When above 30 °C, further raising the temperature resulted in lower beam-to-diffuse transmittance but higher beam-to-diffuse reflectance ($\rho_{f,bd,l}$, $\rho_{b,bd,l}$). Meanwhile, the beam-to-specular reflectance ($\rho_{f,bs,l}$, $\rho_{b,bs,l}$) remained constant, due to the

Table 3
Calculated total transmittance and reflectance of the three window systems from LBNL WINDOW.

Window system		Average visible optical properties			Solar optical properties		
		Transmittance	Front reflectance	Back reflectance	Transmittance	Front reflectance	Back reflectance
BIPV smart window	25 °C	0.698	0.156	0.161	0.520	0.184	0.218
	28 °C	0.558	0.200	0.183	0.422	0.220	0.234
	30 °C	0.349	0.129	0.133	0.278	0.151	0.204
	36 °C	0.105	0.300	0.287	0.086	0.265	0.299
	48 °C	0.074	0.376	0.353	0.055	0.333	0.344
Counterpart BIPV window		0.710	0.137	0.145	0.567	0.223	0.211
Low-e double-glazing		0.814	0.131	0.131	0.641	0.226	0.200

Table 4
U-value of the three window systems.

	U-value (W/m²·K)	
	Manual calculation (EN 673:2011 and ISO 10077–1:2006)	LBNL WINDOW (ISO 15099:2003)
BIPV smart window	1.76	1.75
Counterpart BIPV window	1.77	1.76
Low-e double glazing	1.80	1.78

specular reflections at the glass-air and glass-coating interfaces.

In the next step, the laminate's optical properties were imported to LBNL WINDOW (version 7.6) to generate a BSDF file for the BIPV smart window system. The BSDF file contains data blocks to describe the visible and solar reflection and transmission on the front and back surfaces of the window components [10,33]. Each data block contains a 145×145 matrix, including the data of 145 outgoing directions for each of 145 incident directions [10,33]. Table 3 shows the hemispherical transmittance and reflectance of the three window systems, which were calculated from the bi-directional properties by integration over the outgoing hemispheres [33].

2.3.3. Thermal properties of the BIPV smart window

The thermal transmittance (U-value) of the BIPV smart window system can be calculated by Equation (1) following the standards EN673 [36] and ISO 10077–1:2006 [44]. The thermal conductivities (k_j) of the window's solid layers including the PV encapsulation layer (2 mm), thermotropic layer (1 mm) and glass panes (3 mm) are 0.27, 0.59 and 1.0 W/m·K, respectively. The thermal resistance (R_{air}) of the air gap between the laminate and low-e glass can be assumed as 0.38 m² K/W, given that the air gap is 12 mm thick and adjacent to a coated glass with an emissivity of 0.1 [44]. The thermal resistances of the window's external surface (R_{se}) and internal surface (R_{si}) can be assumed as 0.13 and 0.04 m² K/W, respectively, given that the window is vertically inclined and the emissivities of the external and internal surfaces are greater than 0.8 [44]. Table 4 shows the U-values of the three window systems obtained by manual calculation and from LBNL WINDOW based on ISO 15099:2003 [45].

$$U_g = \frac{1}{R_{se} + \sum_i \frac{d_i}{k_i} + R_{air} + R_{si}} \quad (1)$$

where R_{se} and R_{si} are the external and internal surface resistances (m²·K/W), R_{air} is the thermal resistance of the air gap (m²·K/W), d_i is the thickness of the solid layer i (m), k_i is the thermal conductivity of the solid layer i (W/m·K).

2.3.4. Electrical properties of the BIPV smart window

EnergyPlus integrates three different models for PV power simulation: 'Simple model', 'Equivalent one-diode model' and 'Sandia model' [31,46]. All the three models share the same solar geometry model for the incident solar radiation calculation [31,46]. The Simple model employs Equation (2) with only a few user inputs (such as power conversion efficiency) [46] and does not need special tests to obtain a series of empirical coefficients [31], therefore suitable for rapid performance estimation of developed PV modules. However, this model does not consider the impacts of PV cell temperature and solar concentration on the PV power performance.

The Simple model was chosen in this study to predict the electric power output of the proposed BIPV smart window system. To involve the effects of PV cell temperature and solar concentration (due to total internal reflection within the window), Equation (2) was coupled with Equation (3) [47] and Equation (4) [48] to calculate the actual power

Table 5
Input parameters for the PV power calculation algorithm.

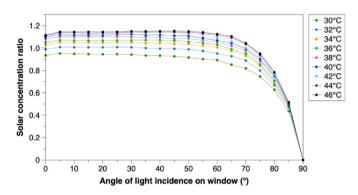| Parameter	value
Window aperture surface area (A_w)	2.25 m²
PV cell coverage ratio (f_{pv})	11%
Power conversion efficiency of the solar cell under STC ($\eta_{pv,STC}$)	17%
Inverter efficiency ($\eta_{inverter}$)	95%
Temperature coefficient of power of the PV cells (ξ)	0.3%/°C

Fig. 7. Predicted solar concentration ratio of the glass-PV-TT-laminate at different thermotropic layer temperatures and angles of light incidence.

conversion efficiency of the PV cells (η_{pv}) and the amount of solar radiation reaching the PV cells (G_{pv}), respectively, while the rest parameters are constant given in Table 5. The solar concentration ratio (C_e), which is defined as the irradiance ratio between the aperture surfaces of the receiver (PV cell) and solar concentrator (glass-PV-TT-glass laminate) [48], can be obtained by the validated ray-tracing method reported in our previous study [23].

Fig. 7 shows the simulated solar concentration ratios of the BIPV smart window system at various TT layer temperatures (between 30 °C and 46 °C) and angles of light incidence on it (between 0° and 90°). At the same TT layer temperatures, the solar concentration ratios were nearly constant over the incidence angle range of 0°–65°, while reducing sharply at larger incidence angles. At the same incidence angles, the solar concentration ratios increased with the TT layer temperature until it reached 44 °C and stabilised upon further heating.

$$P = G_{pv} \times A_w \times f_{pv} \times \eta_{pv} \times \eta_{inverter} \quad (2)$$

$$\eta_{pv} = \eta_{pv,\,STC} \times \left(1 - \xi \times \left(T_{pv} - 25\right)\right) \quad (3)$$

$$G_{pv} = G_w \times C_e \quad (4)$$

where P is the electric power output of the BIPV smart window (W), G_{pv} is the global solar irradiance on the PV cells (W/m²), A_w is the glazing aperture area (m²), f_{pv} is the PV cell coverage ratio, η_{pv} is the actual power conversion efficiency of the PV cells, $\eta_{inverter}$ is the inverter efficiency, $\eta_{pv,STC}$ is the power conversion efficiency of the PV cells under the Standard Test Conditions (STC, viz. 1000 W/m², AM 1.5 global solar irradiation and cell temperature of 25 °C), ξ is the temperature coefficient of power (%/°C), T_{pv} is the PV cell temperature (°C), G_w is the global solar irradiance on the window outside surface (W/m²), C_e is the predicted solar concentration ratio.

The proposed PV power calculation method was validated by comparison with the outdoor experiment results reported in our previous publication [25]. In the previous experiment, a small-scale glass-PV-TT-glass laminate was fabricated and tested in Nottingham under different sky conditions such as clear and partially cloudy. Its instantaneous maximum power outputs can be predicted by Equations (2)–(4), with inputs of solar concentration ratio, solar irradiance, PV cell efficiency and temperature, etc. All the input parameters can be obtained by
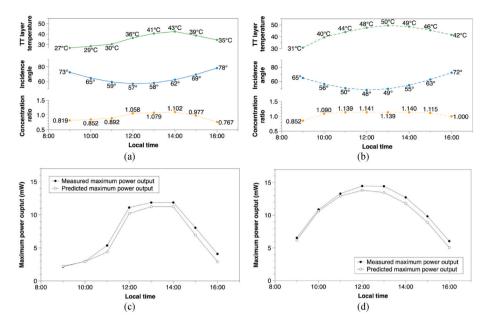
Fig. 8. Predicted solar concentration ratios of the glass-PV-TT-glass laminate sample with the measured TT layer temperatures and calculated solar incidence angles on the dates of (a) July 24, 2019 and (b) August 25, 2019. Comparison between the calculated and measured power outputs of the glass-PV-TT-glass laminate sample on (c) July 24, 2019 and (d) August 25, 2019.

Table 6
Simulation parameters for a UK cellular office.

Parameters		Benchmark range for building performance simulation [51]	Values used in this study
U-value (W/m² K)	Walls	≤0.35	0.35
	Roofs	≤0.25	0.25
	Windows	≤2.2	≤1.8
Heating temperature setpoint (°C)		20–23	20
Cooling temperature setpoint (°C)		23–26	26
Maximum occupant density (m²/person)		6–15	9
Infiltration rate (ACH)		0.16–1.0	0.5
Equipment heat gain (W/m²)		10–25	15
Lighting power density (W/m²)		4–24	9
Illuminance over a task area (lux)		300–500	300

measurements except the solar concentration ratio, which can be predicted from Fig. 7 according to the TT layer temperature (by measurements) and the angle of solar incidence on the laminate sample (by calculations). The angle of solar incidence can be derived by the equations in Appendix C. Fig. 8 shows the predicted solar concentration ratios and instantaneous maximum power outputs at specific times of the test days (July 24th and August 25th, 2019). It can be seen that the predicted maximum power outputs of the laminate sample are in good agreement with the experimental observations.

2.4. Other settings in the BPS model

EnergyPlus (version 9.4) was used for the building performance simulation. In the model setup, the boundary conditions of the south wall and horizontal roof of the office room were set as 'exposed to the outdoor environment', and those of the rest walls and floor were set as 'adiabatic' (i.e., no heat transfer through them). Table 6 shows the U-values specified for the building elements in EnergyPlus, compared to the maximum allowed U-values for office buildings in the UK under the latest Building Regulation Part L2A [49]. The office room was assumed

to be occupied by one person from 9:00 to 17:00 on weekdays all year long. An ideal-load HVAC system with a dual setpoint control was used to maintain the indoor air temperature between 20 °C and 26 °C, which is compliant with the recommended HVAC design temperatures for office buildings by the Chartered Institution of Building Services Engineers (CIBSE) [50]. The internal heat gain from electric equipment and the lighting power density were assumed to be 15 W/m² and 9 W/m², respectively. The electric lighting was set to be automatically controlled. Specifically, during the working hours, the electric lighting was switched on once the daylight illuminance over the task area (located at the centre of the office room with a 0.75 m height above the floor) fell below 300 lux.

To achieve the timely adjustment of the electrical and optical properties of the BIPV smart window, the Energy Management System (EMS) tool available in EnergyPlus was employed. The EMS consists of sensors, actuators and user-defined control algorithms which are written in a simplified programming language called EnergyPlus Runtime Language (ERL) [52]. Favoino et al. (2015) has investigated the reliability of the EMS and found a good agreement between the simulated and measured results for a thermotropic triple glazing unit mounted on an outdoor test facility [52]. In this study, the EMS adjusted the window's electrical properties by changing the values of solar concentration ratio and PV cell efficiency in the aforementioned algorithm for PV power calculation (Equations (2)–(4)), and adjusted the window's optical properties by substituting the window construction with another and using a different dataset of BSDF properties, according to the data from sensors (including window surface temperature and solar incidence angle cosine value). The relevant ERL code is given in Appendix D. The reliability of the EnergyPlus program and the EMS modelling approach has been validated by using the ANSI/ASHRAE 140 standard [53] and comparing with other similar models under the same conditions (see Appendix E). Validation of the EnergyPlus simulation method for a BIPV window using measured data has been demonstrated in the author's previous publication [54].

3. Results and discussion

In this section, the simulation results for the thermal, energy and daylight performance of the office room under the climatic condition of
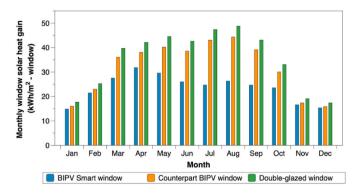
Fig. 9. Monthly solar heat gains (kWh per window area) through the three glazing systems.
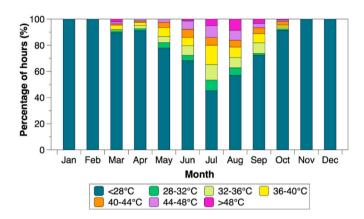

Fig. 10. Percentage of working hours (range: 9:00–17:00) where the thermotropic layer has a temperature within the specific ranges.

Nottingham (the UK) are presented. The effects of using the proposed BIPV smart window system are discussed from the perspectives of window solar heat gain, energy generation and consumption (for heating, cooling and artificial lighting), and daylight availability. Finally, a comparative analysis is carried out to elucidate the influence of different window design scenarios, including WWR, orientation and TT transition temperature.

3.1. Window solar heat gain

Fig. 9 shows the monthly solar heat gains through the BIPV smart window, counterpart BIPV window and low-e double-glazed window when applied in the office room with a WWR of 25% and south glazing orientation. As can be seen, both BIPV windows allow less solar heat to be admitted to the indoor space when compared with the low-e double-glazed window. This occurs probably because a portion of incident solar radiation is absorbed and converted to electricity by the integrated PV cells. During the cold months of November to February, the solar heat gains through the BIPV smart window are slightly lower than those through the counterpart BIPV window, due to its slightly lower solar transmittance when the TT layer temperature is below 28 °C. This fact is revealed in Fig. 10 and Table 3. During the warm months of March to October, significant reductions in solar heat gain are observed for the BIPV smart window over the counterpart BIPV window. Take the hottest month July as an example: using the BIPV smart window can reduce the monthly solar heat gain through window by 41.8% compared to the counterpart BIPV window and 47.1% compared to the low-e double-glazed window. This is likely attributed to the large percentages of hours during summer where the TT layer reaches temperatures above 28 °C (see Fig. 10), resulting in significant reductions of the solar transmittance of the BIPV smart window (see Table 3).

3.2. Energy consumption and electricity generation

Fig. 11 shows a comparison of the monthly heating, cooling and artificial lighting loads of the office room when using the different window systems. From March to October, using the BIPV smart window results in the lowest monthly cooling loads, followed by the counterpart BIPV window and the low-e double-glazed window. From November to March, the monthly heating loads of the office room are slightly increased by using the BIPV smart window. These differences can be explained by the finding in **Section 3.1**, that is, the BIPV smart window effectively reduces the monthly solar heat gains in the office room in summer, thus contributing to lower cooling energy consumption; on the other hand, the BIPV smart window integrates a TT layer (semi-transparent) and PV cells (opaque) which reduce the transmission of useful sunlight for space heating in winter. The monthly artificial lighting loads are also slightly increased by using the BIPV smart window. This is because during a hot period, the BIPV smart window works as a shading device and blocks visible light into the space, and therefore artificial lighting is required to be switched on to maintain a desired indoor
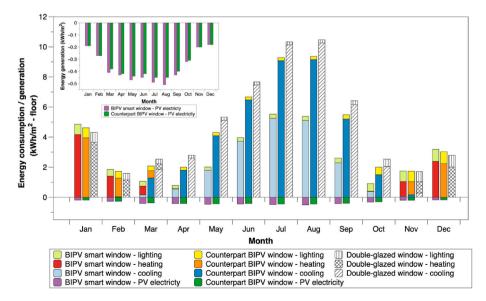

Fig. 11. Comparison of the monthly energy consumption and generation (kWh per floor area) of the office room when installed with the different window systems.

Table 7
Annual energy consumption and generation of the office room.

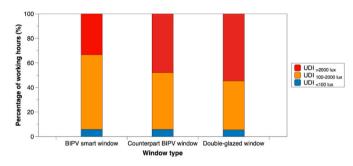|	Annual Cooling (kWh/m²)	Annual Heating (kWh/m²)	Annual Lighting (kWh/m²)	Annual PV electricity (kWh/m²)	Annual net Energy use (kWh/m²)
BIPV Smart window	20.2	9.6	5.0	4.3	30.5
Counterpart BIPV window	38.8	8.8	4.7	4.1	48.2
Low-e double-glazed window	46.0	7.8	4.6	0.0	58.4

Fig. 12. Annual UDI distribution in the office room with a south-facing window and a WWR of 25%.

illuminance level.

Apart from saving energy for space cooling, the BIPV smart window can generate more electricity than the counterpart BIPV window, as shown in Fig. 11. The difference in monthly electric energy output between the BIPV smart window and its counterpart system becomes larger as the weather warms up, reaching a maximum of approximately 10% in August. This could be explained by the data in Fig. 10 that the BIPV smart window maintains in its scattering state (above 28 °C) over a longer period during summer than during winter, as a result of which the solar concentration effect becomes more prominent (see Fig. 7) and thus improves the PV power output.

Table 7 shows the annual energy performance of the office room when installed with the different window systems. Both BIPV windows contribute to lower annual cooling loads, but higher annual heating loads and lighting loads, compared to the low-e double-glazed window. However, the BIPV smart window outperforms the counterpart BIPV window with a reduction in annual cooling load by 18.5 kWh/m² and an

increase in annual electricity generation by 0.2 kWh/m². The BIPV smart window offers annual net energy savings of 36.6% compared to the counterpart BIPV window and 47.7% compared to the low-e double-glazed window.

3.3. Daylight performance

To assess daylight availability in the building interior, Useful Daylight Illuminance (UDI) is generally used as the performance metric. In this study, the percentages of annual working hours when the daylight illuminance on the working plane falls within three standard UDI bins were predicted. The working plane was assumed to be at the centre of the room and a height of 0.75 m above the floor. The UDI bins include (1) an undersupply UDI bin where the hourly illuminances are lower than 100 lux (labelled as 'UDI$_{<100 \text{ lux}}$'); (2) an oversupply UDI bin where the hourly illuminances exceed 2000 lux (labelled as 'UDI$_{>2000 \text{ lux}}$'); (3) a useful bin where the hourly illuminances are in the range of 100–2000 lux (labelled as 'UDI$_{100–2000 \text{ lux}}$') [37,41]. Periods that fall into the UDI$_{<100 \text{ lux}}$ and UDI$_{>2000 \text{ lux}}$ bins often encourage some form of intervention, since the undersupply of daylight (UDI$_{<100 \text{ lux}}$) could lead to an increased demand for supplementary artificial lighting, while the oversupply of daylight (UDI$_{>2000 \text{ lux}}$) is likely to cause visual discomfort of occupants. Periods that lands in the UDI$_{100–2000 \text{ lux}}$ bin generally require neither electric lighting nor solar shading, and it may be assumed that the luminous environment meets the needs of occupants.

Fig. 12 shows the annual UDI distribution for the different window types. For the low-e double-glazed window, the periods when the office is exposed to oversupplied daylight (UDI$_{>2000 \text{ lux}}$), undersupplied daylight (UDI$_{<100 \text{ lux}}$) and desirable illumination (UDI$_{100–2000 \text{ lux}}$) account for 54.6%, 5.4% and 39.9%, respectively. The percentage of UDI$_{100–2000 \text{ lux}}$ is slightly increased to 46.4% when the counterpart BIPV window is used. In contrast, using the BIPV smart window significantly raises the percentage of UDI$_{100–2000 \text{ lux}}$ to 60.9% with a lower risk of over-illumination (i.e., the percentage of UDI$_{>2000 \text{ lux}}$ is 33.3%). This can be attributed to the shading effect imposed by the BIPV smart window, which is minimal in cold periods but significant in hot periods. This is confirmed in Fig. 13, which shows the hourly variations of illuminance in the office room during cold and hot days. From Fig. 13 (a), similar hourly illuminances are observed for the three windows during the winter day, because of the low window temperatures. From Fig. 13 (b), it can be seen that the BIPV smart window yields considerably lower hourly illuminances than the reference windows during the hot periods (10:00–18:00) of the summer day (Fig. 13 (b)). The above results suggest the effective daylighting control ability of the BIPV smart window.

3.4. Effect of window orientation and WWR

Further simulations have been carried out to examine the effects of
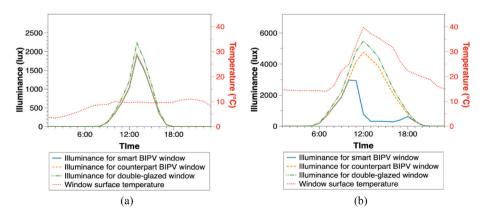

(a)

(b)

Fig. 13. Comparison of the hourly illuminance in the office room when installed with the different window systems on (a) a winter day (January 31st) and (b) a summer day (July 31st).
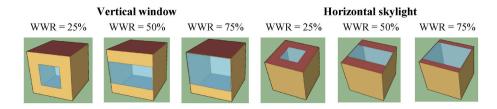
Vertical window

WWR = 25%   WWR = 50%   WWR = 75%

Horizontal skylight

WWR = 25%   WWR = 50%   WWR = 75%

Fig. 14. Diagrams of the office room using different window-to-wall ratios (WWR) for the south/west/east-facing window and horizontal roof skylight.
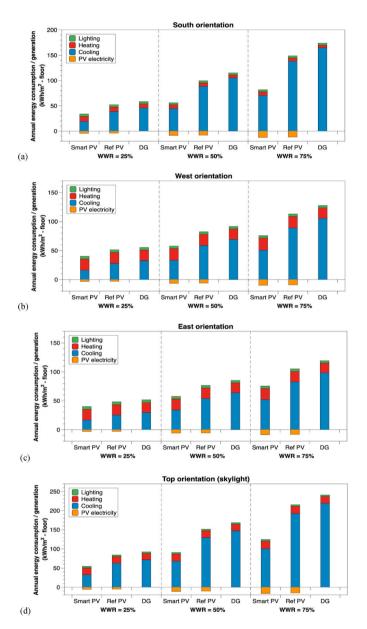

Fig. 15. Annual energy use and generation for the (a) south-facing windows, (b) west-facing windows, (c) east-facing windows and (d) horizontal skylight under different WWRs.

different window orientations and WWRs on the window performance. Four orientations including south, west, east and top (horizontal skylight) were considered in the EnergyPlus simulations. In each orientation group, three WWRs were considered: 25%, 50% and 75% (see Fig. 14), which are recommended to represent the low, medium and high levels of glazing coverage in an office building, respectively [51]. Therefore, 12 architecture design scenarios in total were numerically

investigated.

The predicted annual energy consumption and generation for different window orientations and WWRs are shown in Fig. 15. Under the same WWRs, all the window types with the top orientation show the highest annual cooling loads, followed by the south, west and east orientations. This may be because the horizontal skylights receive more solar radiation than the vertical windows in hot seasons due to high solar elevation angles. Under the same WWRs, the south orientation cases require the lowest amounts of heating energy, due to the longest exposure to direct solar radiation in cold seasons because of low solar elevation angles. Under the same orientations, increasing the WWR from 25% to 75% can cause the increase of annual cooling loads, but also contribute to more PV electricity generated.

From Table 8, it can be seen that the top orientation (skylight) is associated with the largest net energy consumption among the four orientations, regardless of WWR. On the other hand, the office room with a larger WWR consumes more energy annually, regardless of glazing orientation. Amongst the different window types, the BIPV smart window exhibits the lowest annual net energy consumption in all cases of orientation and WWR. Take the office room with a skylight with a WWR of 75% as an example: the annual energy savings provided by the BIPV smart window and the counterpart BIPV window are 55.2% and 16.8%, respectively, compared to the low-e double-glazed window. In terms of daylight performance, as can be seen from Table 9, the office room with the BIPV smart window has the largest percentages of annual working hours when the desired daylight illumination levels (between 100 and 2000 lux) have occurred. This finding is consistent for all the selected orientations and WWRs.

Overall, the results suggest that using the BIPV smart window in place of the traditional BIPV window or low-e double-glazed window can improve both overall energy efficiency and indoor luminous environment for the office room with the selected glazing orientations and WWRs.

3.5. Effect of transition temperature

To better take advantage of the BIPV smart window for energy saving and daylighting control, this section takes a more in-depth look at how the window performance is affected by the transition temperature of the thermotropic layer. A series of EnergyPlus models with the same setups as the previous model (i.e. an office room with south orientation and 25% WWR), except the transition temperature for the BIPV smart window, have been developed for the comparative analysis. The transition temperature was varied in the range of 20 °C–40 °C with an interval of 2 °C. For simplicity, the optical and electrical properties of the BIPV smart window derived for the transition temperature of 30 °C (abbreviated as 'TT30') were used in the new models. The only difference is that the window's property data were shifted to the transition temperature under testing, for example, the BSDF properties assigned to the TT layer temperatures of 26 °C and 40 °C in the TT30 model were assigned to the TT layer temperatures of 28 °C and 42 °C in the TT32 model.

Fig. 16 shows the predicted annual energy consumption and electricity generation for different transition temperatures. It can be clearly seen that by reducing the transition temperature from 40 °C to 20 °C, the annual cooling load of the office room decreases, but in the meantime, the annual heating and lighting loads increase. Moreover, the annual

Table 8
Annual net energy consumption for different WWRs and orientations. The values in brackets are the annual net energy savings relative to the low-e double-glazed window (DG).

	South window (kWh/m² - floor)			West window (kWh/m² - floor)			East window (kWh/m² - floor)			Horizontal skylight (kWh/m² - floor)		
	Smart	Ref	DG	Smart	Ref	DG	Smart	Ref	DG	Smart	Ref	DG
WWR = 25%	30.5 (47.7%)	48.2 (17.5%)	58.4	37.0 (32.9%)	48.4 (12.3%)	55.2	37.1 (28.3%)	45.3 (12.4%)	51.7	49.1 (46.8%)	79.1 (14.4%)	92.3
WWR = 50%	47.9 (58.5%)	91.7 (20.4%)	115.3	51.3 (44.0%)	76.3 (16.7%)	91.6	51.6 (39.5%)	70.9 (16.9%)	85.3	79.8 (52.6%)	141.3 (16.2%)	168.5
WWR = 75%	69.3 (60.1%)	137.1 (21.2%)	174.0	65.9 (48.4%)	103.7 (18.8%)	127.7	66.7 (44.2%)	96.8 (18.9%)	119.4	108.0 (55.2%)	200.3 (16.8%)	240.9

Table 9
Percentages of annual working hours when the daylight illuminance in the office room lands in the $UDI_{100-2000}$ bin for different WWRs and glazing orientations.

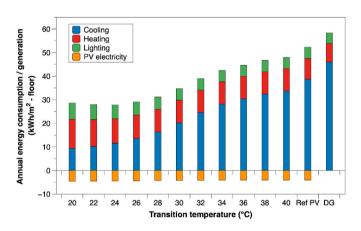|	South window			West window			East window			Horizontal skylight		
	Smart	Ref	DG	Smart	Ref	DG	Smart	Ref	DG	Smart	Ref	DG
WWR = 25%	60.9%	46.4%	39.9%	80.6%	70.9%	67.2%	78.3%	73.4%	69.1%	63.0%	47.0%	41.6%
WWR = 50%	47.2%	28.3%	24.8%	63.0%	54.6%	48.1%	64.8%	57.0%	51.5%	45.3%	28.2%	23.5%
WWR = 75%	40.3%	21.0%	18.1%	47.2%	39.3%	32.8%	52.9%	43.2%	36.0%	36.3%	18.8%	16.1%

Fig. 16. Annual energy consumption and on-site electricity generation for the BIPV smart window with different transition temperatures (from 20 °C to 40 °C), the counterpart BIPV window (Ref PV) and the low-e double-glazed window (DG).

electricity generation by the BIPV smart window slightly increases when using a lower transition temperature. As can be seen from Table 10, the annual energy saving by using the BIPV smart window over the low-e double-glazed window increases from 25.0% to 60.0% when the transition temperature is reduced from 40 °C to 24 °C. A slight reduction in annual energy saving is observed by further decreasing the transition temperature to 20 °C. In the perspective of daylight availability, the application of the BIPV smart window with a lower transition temperature contributes to an increased percentage of annual working hours where the daylight illuminance is within the desirable range ($UDI_{100-2000 lux}$). These results suggest that using a lower transition temperature is beneficial for improving the on-site electricity generation, cooling energy saving as well as the luminous environment in the office,

however, possibly causing higher demands for heating and electric lighting. This can be explained because, with a lower transition temperature, the BIPV smart window has transitioned to its translucent state over a longer period across the year, which reduces the cooling demand and the occurrence of over-illumination, enhances the solar concentration effect, and in turn impacts on the gain of useful solar energy for space heating and lighting.

4. Conclusions and recommendations for future work

In this paper, a comprehensive simulation method has been developed to evaluate the performance of a novel BIPV smart window system when applied in buildings. The proposed system was designed consisting of a glass-PV-TT-glass laminate (front cover), an air gap and a low-e glass pane (rear cover). In the system, a hydroxypropyl-cellulose-based thermotropic (TT) hydrogel membrane with a transition temperature of approximately 30 °C was incorporated to achieve the adaptive changes of the window solar heat gain and visible transmittance in response to varying ambient conditions. A systematic modelling workflow has been developed, including the main steps: (1) measuring the TT membrane's thermo-optical properties, (2) predicting and validating the optical, thermal and electrical properties of the proposed BIPV smart window, (3) coupling the window properties with an EnergyPlus model via the Energy Management System (EMS) function, (4) simulating the overall energy and daylight performance of the BIPV smart window in an office-type environment under the climatic condition of Nottingham, the UK. To gain a comprehensive picture of how the building performance is affected by the window in different design scenarios, simulations have been carried out under the selected WWRs (25%, 50% and 75%), glazing orientations (south, west, east and top) and TT transition temperatures (from 20 °C to 40 °C). The following conclusions can be drawn:

Table 10
Window performance with respect to different transition temperatures of the thermotropic layer.

	BIPV smart window											Ref PV	DG
Transition temperature	20 °C	22 °C	24 °C	26 °C	28 °C	30 °C	32 °C	34 °C	36 °C	38 °C	40 °C		
Annual PV electricity (kWh/m²)	4.6	4.5	4.4	4.4	4.3	4.3	4.2	4.2	4.1	4.1	4.1	4.1	/
Annual energy Saving[a]	58.8%	59.9%	60.0%	57.7%	54.0%	47.7%	40.5%	34.5%	30.6%	27.1%	25.0%	17.5%	/
$UDI_{100-2000}$	82.6%	79.5%	75.4%	71.0%	65.8%	60.9%	56.4%	53.1%	51.2%	49.4%	48.5%	46.4%	39.9%

[a] Reduction of net energy consumption compared to the low-e double-glazed window (DG).

1) For the south-oriented office room with a WWR of 25%, using the BIPV smart window can offer a 36.6% reduction in annual net energy consumption, compared to the counterpart BIPV window that has no thermotropic layer integrated. The annual energy saving provided by the BIPV smart window can reach 47.7%, compared to an ordinary low-e double glazing.

2) The percentage of annual working hours when the office room has a desired daylight illuminance level ($UDI_{100-2000 \, lux}$) is 39.9% for the low-e double glazing, which can be improved to 46.4% when using the counterpart BIPV window, and further to 60.9% when using the smart BIPV window.

3) When the WWR of the south-oriented office room is increased from 25% to 75%, the annual energy saving offered by the BIPV smart window over the low-e double glazing can be increased from 47.7% to 60.1%. Similar findings were observed for the top (skylight), west and east orientations.

4) Decreasing the transition temperature of the BIPV smart window system can potentially lead to a lower cooling load, higher electricity output and increased percentage of $UDI_{100-2000 \, lux}$ in the office room. Nevertheless, the transition temperature is not recommended to be decreased further to below 24 °C, due to minimal difference in energy-saving and undesired blockage of useful sunlight and visual connection to the outdoors.

Overall, the BIPV smart window system shows great potential in improving both building energy performance and indoor luminous environment conditions. For practical applications, the proposed system can be fitted in areas such as glass atrium roofs, canopies and glazed façades which consist of spandrel glass and vision glass, where a permanent view from the inside out is not required.

Future work will be devoted to improving the accuracy of the proposed optical, thermal, and electrical models for characterising the dynamic window properties. A long-term, full-scale outdoor experimental campaign will be conducted to further prove the feasibility of the proposed algorithm for PV window power calculation and the EnergyPlus models. The long-term stability and weatherability of the BIPV smart window such as resistances to UV radiation, freezing and microorganism will also be investigated in future experiments. A more comprehensive daylight analysis via RADIANCE will be carried out to evaluate the effectiveness of the proposed system in improving visual comfort across a range of indicators such as UDI, daylight uniformity and Daylight Glare Probability (DGP).

CRediT authorship contribution statement

Xiao Liu: Writing – original draft, Methodology, Investigation, Data curation. **Yupeng Wu:** Writing – review & editing, Supervision, Methodology, Funding acquisition.

Declaration of competing interest

The authors declare that they have no known competing financial interests or personal relationships that could have appeared to influence the work reported in this paper.

Acknowledgements

Appendix A. Optics of a composite film consisting of a scattering film applied over a clear substrate

The optical model from Laouadi and Parekh [32] was developed for estimating the optical properties of composite films (**Appendix A**) or laminated glazings (**Appendix B**) containing scattering films. The optical model is also applicable for composite films or laminates with a pattern structure, i.e., consisting of discrete homogeneous regions, each of which can be made up of stacked layers, for example, c-Si cell PV glazing. The optical properties of the composite film or laminate are calculated based on the net radiation method (i.e., using the flux balance at the interface between two media) and requiring the input of the optical properties of the scattering film when applied over a substrate or within a laminate. However, these input properties are usually not available. An approximation can be made if the bulk scattering of the scattering film dominates its surface scattering, so that the measured optical properties of the scattering film in the free-standing form can be directly used for the calculation [32]. The front transmittance and reflectance of a composite film are calculated by **Equations A1-A4**, and its back transmittance and reflectance are calculated by **Equations A5-A8**.

- Front beam-to-specular transmittance of the composite film ($\tau_{f,bs,c}$)

$$\tau_{f,bs,c} = \frac{(1 - r_s) \bullet t_s \bullet \tau_{f,bs,i}}{1 - \rho_{f,bs,i} \bullet r_s \bullet t_s^2} \tag{A1}$$

- Front beam-to-diffuse transmittance of the composite film ($\tau_{f,bd,c}$)

$$\tau_{f,bd,c} = \frac{(1 - r_s) \bullet t_s}{1 - \rho_{f,bs,i} \bullet r_s \bullet t_s^2} \bullet \left(\tau_{f,bd,i} + \frac{\tau_{f,d,i} \bullet \rho_{f,bd,i} \bullet \left\{ r_s \bullet t_s^2 \right\}_d}{1 - \rho_{f,d,i} \bullet \left\{ r_s \bullet t_s^2 \right\}_d} \right) \tag{A2}$$

- Front beam-to-specular reflectance of the composite film ($\rho_{f,bs,c}$)

$$\rho_{f,bs,c} = r_s + \frac{\rho_{f,bs,i} \bullet (1 - r_s)^2 \bullet t_s^2}{1 - \rho_{f,bs,i} \bullet r_s \bullet t_s^2} \tag{A3}$$

- Front beam-to-diffuse reflectance of the composite film ($\rho_{f,bd,c}$)

$$\rho_{f,bd,c} = \frac{\rho_{f,bd,i} \bullet (1 - r_s) \bullet t_s \bullet \{t_s \bullet (1 - r_s)\}_d}{(1 - \rho_{f,bs,i} \bullet r_s \bullet t_s^2) \bullet (1 - \rho_{f,d,i} \bullet \{r_s \bullet t_s^2\}_d)} \tag{A4}$$

where $\tau_{f,bs,i}$ is the front beam-to-specular transmittance of the scattering layer, $\rho_{f,bs,i}$ is the front beam-to-specular reflectance of the scattering layer, $\tau_{f,bd,i}$ is the front beam-to-diffuse transmittance of the scattering layer, $\rho_{f,bd,i}$ is the front beam-to-diffuse reflectance of the scattering layer, $\tau_{f,d,i}$ is the front diffuse-to-diffuse transmittance of the scattering layer, $\rho_{f,d,i}$ is the front diffuse-to-diffuse reflectance of the scattering layer.

- Back beam-to-specular transmittance of the composite film ($\tau_{b,bs,c}$)

$$\tau_{b,bs,c} = \frac{t_s \bullet (1 - r_s) \bullet \tau_{b,bs,i}}{1 - \rho_{f,bs,i} \bullet r_s \bullet t_s^2} \tag{A5}$$

- Back beam-to-diffuse transmittance of the composite film ($\tau_{b,bd,c}$)

$$\tau_{b,bd,c} = \frac{\{t_s \bullet (1 - r_s)\}_d \bullet \left(\tau_{b,bd,i} + \frac{\tau_{b,bs,i} \bullet \rho_{f,bd,i} \bullet r_s \bullet t_s^2}{1 - \rho_{f,bs,i} \bullet r_s \bullet t_s^2}\right)}{1 - \rho_{f,d,i} \bullet \{t_s\}_d \bullet \{r_s \bullet t_s\}_d} \tag{A6}$$

- Back beam-to-specular reflectance of the composite film ($\rho_{b,bs,c}$)

$$\rho_{b,bs,c} = \rho_{b,bs,i} + \frac{\tau_{f,bs,i} \bullet \tau_{b,bs,i} \bullet r_s \bullet t_s^2}{1 - \rho_{f,bs,i} \bullet r_s \bullet t_s^2} \tag{A7}$$

- Back beam-to-diffuse reflectance of the composite film ($\rho_{b,bd,c}$)

$$\rho_{b,bd,c} = \rho_{b,bd,i} + \frac{\tau_{f,bd,i} \bullet \tau_{b,bs,i} \bullet r_s \bullet t_s^2}{1 - \rho_{f,bs,i} \bullet r_s \bullet t_s^2} + \frac{\tau_{f,d,i} \bullet \{t_s\}_d \bullet \{r_s \bullet t_s\}_d \bullet \left(\tau_{b,bd,i} + \frac{\tau_{b,bs,i} \bullet \rho_{f,bd,i} \bullet r_s \bullet t_s^2}{1 - \rho_{f,bs,i} \bullet r_s \bullet t_s^2}\right)}{1 - \rho_{f,d,i} \bullet \{t_s\}_d \bullet \{r_s \bullet t_s\}_d} \tag{A8}$$

where $\tau_{b,bs,i}$ is the back beam-to-specular transmittance of the scattering layer, $\rho_{b,bs,i}$ is the back beam-to-specular reflectance of the scattering layer, $\tau_{b,bd,i}$ is the back beam-to-diffuse transmittance of the scattering layer, $\rho_{b,bd,i}$ is the back beam-to-diffuse reflectance of the scattering layer, $\tau_{b,d,i}$ is the back diffuse-to-diffuse transmittance of the scattering layer, $\rho_{b,d,i}$ is the back diffuse-to-diffuse reflectance of the scattering layer.

- Angle dependent reflectivity at the interface between media ($r_s(\theta)$)

$$r_s(\theta) = 0.5 \bullet \left[\frac{\sin^2(\varphi - \theta)}{\sin^2(\varphi + \theta)} + \frac{\tan^2(\varphi - \theta)}{\tan^2(\varphi + \theta)}\right] \tag{A9}$$

$$r_s(0) = \left(\frac{n_1 - n_2}{n_1 + n_2}\right)^2 \tag{A10}$$

$$n_1 \sin \theta = n_2 \sin \varphi \tag{A11}$$

where θ is the incident light angle at the interface, φ is the refracted light angle at the interface, n_1 is the refractive index of medium 1, n_2 is the refractive index of medium 2.
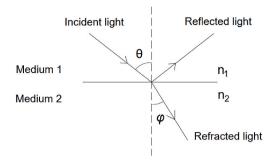
Fig. A1. Light transfer at the interface between two media.

- Transmissivity of the clear substrate (t_s)

$$t_s = e^{-\left(\frac{4\pi \bullet k_s}{\lambda} \bullet \frac{d_s}{\cos \varphi}\right)} \tag{A12}$$

$$t_s = e^{-\left(\alpha_s \bullet \frac{d_s}{\cos \varphi}\right)} \tag{A13}$$

where k_s is the extinction coefficient of the substrate, d_s is the thickness of the substrate, λ is the wavelength of light, α_s is the absorption coefficient of the substrate.

- Diffuse property of the product ($r_s^p \times t_s^q$)

$$\left\{r_s^p \bullet t_s^q\right\}_d = \int_0^{\pi/2} \left[r_s^p(\theta) \bullet t_s^q(\theta)\right] \bullet \sin 2\theta \bullet d\theta \tag{A14}$$

where p and q are ad-hoc exponents. A numerical integration method can be used for the calculation.

- Transmittance (τ_c) and reflectance (ρ_c) of a composite film with discrete homogenous regions

$$\tau_c = \sum_{j=1}^{m} \varepsilon_j \bullet \tau_{c,j} \tag{A15}$$

$$\rho_c = \sum_{j=1}^{m} \varepsilon_j \bullet \rho_{c,j} \tag{A16}$$

where ε_j is the surface fraction of a given homogeneous region (j) with respect to the total pane surface, $\tau_{c,j}$ is the transmittance of the homogeneous region (j), $\rho_{c,j}$ is the transmittance of the homogeneous region (j), m is the number of discrete homogeneous regions.

Appendix B. Optics of a laminated glazing consisting of a composite film between two equal-thickness clear substrates

The front transmittance and reflectance of a laminate are calculated by Equations B1-B4. Its back transmittance and reflectance can also be calculated using the equations, just by swapping the values of the front and back properties of the composite film, for example, the value of $\tau_{f,bs,c}$ is swapped with that of $\tau_{b,bs,c}$. The optical properties of the composite film can be measured or derived from Appendix A.

- Front beam-to-specular transmittance of the laminate ($\tau_{f,bs,l}$)

$$\tau_{f,bs,l} = \frac{\tau_{f,bs,c} \bullet t_s^2 \bullet (1 - r_s)^2}{\left(1 - \rho_{f,bs,c} \bullet r_s \bullet t_s^2\right) \bullet \left(1 - \rho_{b,bs,c} \bullet r_s \bullet t_s^2\right) - \tau_{f,bs,c} \bullet \tau_{b,bs,c} \bullet r_s^2 \bullet t_s^4} \tag{B1}$$

- Front beam-to-diffuse transmittance of the laminate ($\tau_{f,bd,l}$)

$$\tau_{f,bd,l} = t_s \bullet (1 - r_s) \bullet \{t_s \bullet (1 - r_s)\}_d \bullet \frac{\left(1 - \rho_{f,d,c} \bullet \{r_s \bullet t_s^2\}_d\right) \bullet \left(\tau_{f,bd,c} + t_s^2 \bullet r_s \bullet A\right) + \tau_{f,d,c} \bullet \{r_s \bullet t_s^2\}_d \bullet \left(\rho_{f,bd,c} + t_s^2 \bullet r_s \bullet B\right)}{\left(1 - \rho_{b,d,c} \bullet \{r_s \bullet t_s^2\}_d\right) \bullet \left(1 - \rho_{f,d,c} \bullet \{r_s \bullet t_s^2\}_d\right) - \tau_{f,d,c} \bullet \tau_{b,d,c} \bullet \{r_s \bullet t_s^2\}_d^2} \tag{B2}$$

- Front beam-to-specular reflectance of the laminate ($\rho_{f,bs,l}$)

$$\rho_{f,bs,l} = r_s + \frac{t_s^2 \bullet (1 - r_s)^2 \bullet \left[\rho_{f,bs,c} \bullet \left(1 - \rho_{b,bs,c} \bullet r_s \bullet t_s^2\right) + \tau_{f,bs,c} \bullet \tau_{b,bs,c} \bullet r_s \bullet t_s^2\right]}{\left(1 - \rho_{f,bs,c} \bullet r_s \bullet t_s^2\right) \bullet \left(1 - \rho_{b,bs,c} \bullet r_s \bullet t_s^2\right) - \tau_{f,bs,c} \bullet \tau_{b,bs,c} \bullet r_s^2 \bullet t_s^4} \tag{B3}$$

- Front beam-to-diffuse reflectance of the laminate ($\rho_{f,bd,l}$)

$$\rho_{f,bd,l} = t_s \bullet (1 - r_s) \bullet \{t_s \bullet (1 - r_s)\}_d \bullet \frac{\left(1 - \rho_{b,d,c} \bullet \{r_s \bullet t_s^2\}_d\right) \bullet \left(\rho_{f,bd,c} + t_s^2 \bullet r_s \bullet B\right) + \tau_{b,d,c} \bullet \{r_s \bullet t_s^2\}_d \bullet \left(\tau_{f,bd,c} + t_s^2 \bullet r_s \bullet A\right)}{\left(1 - \rho_{b,d,c} \bullet \{r_s \bullet t_s^2\}_d\right) \bullet \left(1 - \rho_{f,d,c} \bullet \{r_s \bullet t_s^2\}_d\right) - \tau_{f,d,c} \bullet \tau_{b,d,c} \bullet \{r_s \bullet t_s^2\}_d^2} \tag{B4}$$

$$A = \frac{\tau_{f,bd,c} \bullet \left[\rho_{f,bs,c} \bullet \left(1 - \rho_{b,bs,c} \bullet r_s \bullet t_s^2\right) + \tau_{f,bs,c} \bullet \tau_{b,bs,c} \bullet r_s \bullet t_s^2\right] + \rho_{b,bd,c} \bullet \tau_{f,bs,c}}{\left(1 - \rho_{f,bs,c} \bullet r_s \bullet t_s^2\right) \bullet \left(1 - \rho_{b,bs,c} \bullet r_s \bullet t_s^2\right) - \tau_{f,bs,c} \bullet \tau_{b,bs,c} \bullet r_s^2 \bullet t_s^4} \tag{B5}$$

$$B = \frac{\rho_{f,bd,c} \bullet \left[\rho_{f,bs,c} \bullet \left(1 - \rho_{b,bs,c} \bullet r_s \bullet t_s^2\right) + \tau_{f,bs,c} \bullet \tau_{b,bs,c} \bullet r_s \bullet t_s^2\right] + \tau_{b,bd,c} \bullet \tau_{f,bs,c}}{\left(1 - \rho_{f,bs,c} \bullet r_s \bullet t_s^2\right) \bullet \left(1 - \rho_{b,bs,c} \bullet r_s \bullet t_s^2\right) - \tau_{f,bs,c} \bullet \tau_{b,bs,c} \bullet r_s^2 \bullet t_s^4} \tag{B6}$$

where $\tau_{f,bs,c}$ is the front beam-to-specular transmittance of the composite film, $\rho_{f,bs,c}$ is the front beam-to-specular reflectance of the composite film, $\tau_{f,bd,c}$ is the front beam-to-diffuse transmittance of the composite film, $\rho_{f,bd,c}$ is the front beam-to-diffuse reflectance of the composite film, $\tau_{f,d,c}$ is the front diffuse-to-diffuse transmittance of the composite film, $\rho_{f,d,c}$ is the front diffuse-to-diffuse reflectance of the composite film, $\tau_{b,bs,c}$ is the back beam-to-specular transmittance of the composite film, $\rho_{b,bs,c}$ is the back beam-to-specular reflectance of the composite film, $\tau_{b,bd,c}$ is the back beam-to-diffuse transmittance of the composite film, $\rho_{b,bd,c}$ is the back beam-to-diffuse reflectance of the composite film, $\tau_{b,d,c}$ is the back diffuse-to-diffuse transmittance of the composite film, $\rho_{b,d,c}$ is the back diffuse-to-diffuse reflectance of the composite film.

Appendix C. Calculation of the solar incident angle on a surface

The angle of light incidence (θ) on a surface can be calculated by Equation (C1) [55]. It can be simplified to Equation (C2) if the investigated surface is vertically inclined ($\beta = 90°$), facing south and in the northern hemisphere ($Z_s = 0°$) [55], which is the case for the glass-PV-TT-glass laminate in the experimental validation study. In Equation (C2), the local latitude (L) is known, the declination angle (δ) can be calculated by Equation (C3), and the hour angle (h) can be expressed by Equation (C4) (if knowing the solar altitude angle (α) and the solar azimuth angle (z)) or Equation (C5). With the aid of this incidence angle calculation, the solar concentration ratio at a specific time can be determined for PV power calculation and for validation purpose.

$$\cos\theta = \sin(L)\sin(\delta)\cos(\beta) - \cos(L)\sin(\delta)\sin(\beta)\cos(Z_s) + \cos(L)\cos(\delta)\cos(h)\cos(\beta) + \sin(L)\cos(\delta)\cos(h)\sin(\beta)\cos(Z_s) + \cos(\delta)\sin(h)\sin(\beta)\sin(Z_s) \tag{C1}$$

$$\cos\theta = -\cos(L)\sin(\delta) + \sin(L)\cos(\delta)\cos(h) \tag{C2}$$

$$\delta = 23.45 \sin\left[\frac{360}{365}\left(284 + N\right)\right] \tag{C3}$$

$$\sin h = \frac{\cos\alpha\sin(z)}{\cos\delta} \tag{C4}$$

$$h = \pm 0.25 \text{ (Number of minutes from local solar noon)} \tag{C5}$$

where θ is the angle of incidence between the solar beam on a surface and the normal to the surface, δ is the declination angle, L is the local latitude, β is the surface tilt angle, Z_s is the surface azimuth angle, h is the hour angle, N is the day number, α is the solar altitude angle, z is the solar azimuth angle, Φ is the solar zenith angle.
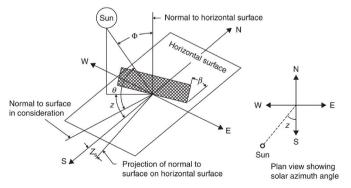

Fig. C1. Diagram of solar radiation incident on a surface. Picture source: [55].

Appendix D. Control Algorithms defined in the EMS

The relevant ERL code is given below. It was assumed that the temperatures of the thermotropic layer and PV cells are equal to the temperature of the window's outside surface in the EnergyPlus model. The window surface temperature and the cosine value of angle of solar incidence on the window were sensed by the EMS to determine the solar concentration ratio (from Fig. 7) for PV power calculation.

(1) The electrical property control algorithm:

> *Set IncidentAngleRad = @ArcCos Solar_Beam_Incident_Cos,*
>
> *Set IncidentAngle = @RadToDeg IncidentAngleRad,*
>
> *IF (Smart_window_temperature_sensor <= 25) && (IncidentAngle <= 60),*
>
> *Set Smart_PV_window_power_output = Simple_model_power_output*0.0948   ! Modify the Simple model by involving the solar concentration effect*
>
> *ELSEIF (Smart_window_temperature_sensor <= 30) && (IncidentAngle <= 60),*
>
> *Set Smart_PV_window_power_output = Simple_model_power_output*(1-0.003* (Smart_window_temperature_sensor-25))*0.0948,   ! Modify the Simple model by involving the temperature effect*
>
> *ELSEIF ……   ! Change the solar concentration ratio for another window surface temperature*
>
> *ELSEIF (Smart_window_temperature_sensor >48) && (IncidentAngle <= 60)*
>
> *Set Smart_PV_window_power_output = Simple_model_power_output*(1-0.003* (Smart_window_temperature_sensor-25))*1.126,*
>
> *ELSEIF ……   ! Change the solar concentration ratio for another solar incidence angle*
>
> *ELSEIF (Smart_window_temperature_sensor >48) && (IncidentAngle > 85)*
>
> *Set Smart_PV_window_power_output = Simple_model_power_output*(1-0.003* (Smart_window_temperature_sensor-25))*0,*
>
> *ENDIF;*

(2) The optical property control algorithm:

> *IF Smart_window_temperature_sensor <= 25,*
>
> *SET Win_Construction = Smart_glazing_T25,   ! Select the complex fenestration state for 25 degree C*
>
> *ELSEIF ……   ! Change the surface construction state for another window surface temperature*
>
> *ELSEIF Smart_window_temperature_sensor <= 48,*
>
> *SET Win_Construction = Smart_glazing_T48,*
>
> *ELSE*
>
> *SET Win_Construction = Smart_glazing_T48,*
>
> *ENDIF;*

Appendix E. Validation of the EnergyPlus simulation method

To validate the EMS modelling approach, EnergyPlus models have been developed under the same conditions (such as building geometry, smart window properties, occupant/equipment schedules and climatic conditions) as described in the study of Tällberg et al. [56]. The results have been compared with the literature data obtained using the software IDA Indoor Climate and Energy (IDA ICE) [56]. From Figure E1, it can be seen that the annual loads of heating, cooling, lighting and equipment of a buidling with thermochromic windows predicted by EnergyPlus are similar to the ones by IDA ICE. The validation provides confidence in the developed method for dynamic window modelling and building performance prediction.
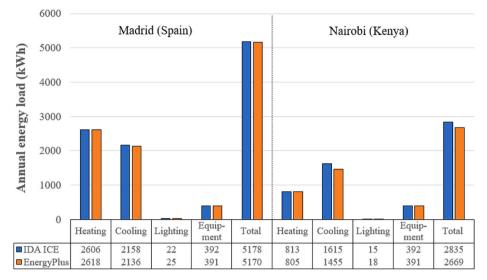
Fig. E1. Comparison of the simulation results between IDA ICE and EnergyPlus for a building with thermochromic windows under the climatic conditions of (a) Madrid (Spain) and (b) Nairobi (Kenya).

References

[1] J.H. Kämpf, M. Montavon, J. Bunyesc, R. Bolliger, D. Robinson, Optimisation of buildings' solar irradiation availability, Sol. Energy 84 (4) (2010) 596–603.

[2] L. Vanhoutteghem, G.C.J. Skarning, C.A. Hviid, S. Svendsen, Impact of façade window design on energy, daylighting and thermal comfort in nearly zero-energy houses, Energy Build. 102 (2015) 149–156.

[3] Y. Fang, T.J. Hyde, F. Arya, N. Hewitt, R. Wang, Y. Dai, Enhancing the thermal performance of triple vacuum glazing with low-emittance coatings, Energy Build. 97 (2015) 186–195.

[4] M. Casini, Active dynamic windows for buildings: a review, Renew. Energy 119 (2018) 923–934.

[5] A. Ghosh, B. Norton, A. Duffy, Measured thermal performance of a combined suspended particle switchable device evacuated glazing, Appl. Energy 169 (2016) 469–480.

[6] Y. Sun, Glazing System with Transparent Insulation Material for Building Energy Saving and Daylight Comfort, University of Nottingham, 2017.

[7] G. Cattarin, F. Causone, A. Kindinis, L. Pagliano, Outdoor test cells for building envelope experimental characterisation-A literature review, Renew. Sustain. Energy Rev. 54 (2016) 606–625.

[8] Y. Sun, R. Liang, Y. Wu, R. Wilson, P. Rutherford, Development of a comprehensive method to analyse glazing systems with Parallel Slat Transparent Insulation material (PS-TIM), Appl. Energy 205 (2017) 951–963.

[9] N. Jakica, State-of-the-art review of solar design tools and methods for assessing daylighting and solar potential for building-integrated photovoltaics, Renew. Sustain. Energy Rev. 81 (2018) 1296–1328.

[10] A. McNeil, C. Jonsson, D. Appelfeld, G. Ward, E.S. Lee, A validation of a ray-tracing tool used to generate bi-directional scattering distribution functions for complex fenestration systems, Sol. Energy 98 (2013) 404–414.

[11] S. Hoffmann, E.S. Lee, C. Clavero, Examination of the technical potential of near-infrared switching thermochromic windows for commercial building applications, Sol. Energy Mater. Sol. Cell. 123 (2014) 65–80.

[12] M.E. Warwick, I. Ridley, R. Binions, The effect of transition gradient in thermochromic glazing systems, Energy Build. 77 (2014) 80–90.

[13] R. Liang, Y. Sun, M. Aburas, R. Wilson, Y. Wu, An exploration of the combined effects of NIR and VIS spectrally selective thermochromic materials on building performance, Energy Build. 201 (2019) 149–162.

[14] M. Aburas, H. Ebendorff-Heidepriem, L. Lei, M. Li, J. Zhao, T. Williamson, Y. Wu, V. Soebarto, Smart windows-Transmittance tuned thermochromic coatings for dynamic control of building performance, Energy Build. 235 (2021) 110717.

[15] M. Aburas, V. Soebarto, T. Williamson, R. Liang, H. Ebendorff-Heidepriem, Y. Wu, Thermochromic smart window technologies for building application: a review, Appl. Energy 255 (2019) 113522.

[16] X.-H. Li, C. Liu, S.-P. Feng, N.X. Fang, Broadband light management with thermochromic hydrogel microparticles for smart windows, Joule 3 (1) (2019) 290–302.

[17] Y. Wu, K. Connelly, Y. Liu, X. Gu, Y. Gao, G.Z. Chen, Smart solar concentrators for building integrated photovoltaic façades, Sol. Energy 133 (2016) 111–118.

[18] K. Connelly, Y. Wu, J. Chen, Y. Lei, Design and development of a reflective membrane for a novel building integrated concentrating photovoltaic (BICPV) 'smart window' system, Appl. Energy 182 (2016) 331–339.

[19] K. Allen, K. Connelly, P. Rutherford, Y. Wu, Smart windows—dynamic control of building energy performance, Energy Build. 139 (2017) 535–546.

[20] T. Jiang, X. Zhao, X. Yin, R. Yang, G. Tan, Dynamically adaptive window design with thermo-responsive hydrogel for energy efficiency, Appl. Energy 287 (2021), 116573.

[21] J. Yao, N. Zhu, Evaluation of indoor thermal environmental, energy and daylighting performance of thermotropic windows, Build. Environ. 49 (2012) 283–290.

[22] K. Connelly, Y. Wu, X. Ma, Y. Lei, Transmittance and reflectance studies of thermotropic material for a novel building integrated concentrating photovoltaic (BICPV) 'Smart Window' System, Energies 10 (11) (2017) 1889.

[23] X. Liu, Y. Wu, Monte-Carlo optical model coupled with Inverse Adding-Doubling for Building Integrated Photovoltaic smart window design and characterisation, Sol. Energy Mater. Sol. Cell. 223 (2021), 110972.

[24] X. Liu, Y. Wu, Design, development and characterisation of a Building Integrated Concentrating Photovoltaic (BICPV) smart window system, Sol. Energy 220 (2021) 722–734.

[25] X. Liu, Y. Wu, Experimental characterisation of a smart glazing with tuneable transparency, light scattering ability and electricity generation function, Appl. Energy 303 (2021), 117521.

[26] W. Zhang, L. Lu, J. Peng, A. Song, Comparison of the overall energy performance of semi-transparent photovoltaic windows and common energy-efficient windows in Hong Kong, Energy Build. 128 (2016) 511–518.

[27] N. Skandalos, D. Karamanis, Investigation of thermal performance of semi-transparent PV technologies, Energy Build. 124 (2016) 19–34.

[28] Y.T. Chae, J. Kim, H. Park, B. Shin, Building energy performance evaluation of building integrated photovoltaic (BIPV) window with semi-transparent solar cells, Appl. Energy 129 (2014) 217–227.

[29] E. Leite Didoné, A. Wagner, Semi-transparent PV windows: a study for office buildings in Brazil, Energy Build. 67 (2013) 136–142.

[30] J. Peng, D.C. Curcija, L. Lu, S.E. Selkowitz, H. Yang, W. Zhang, Numerical investigation of the energy saving potential of a semi-transparent photovoltaic double-skin facade in a cool-summer Mediterranean climate, Appl. Energy 165 (2016) 345–356.

[31] J. Peng, D.C. Curcija, L. Lu, S.E. Selkowitz, H. Yang, R. Mitchell, Developing a method and simulation model for evaluating the overall energy performance of a ventilated semi-transparent photovoltaic double-skin facade, Prog. Photovoltaics Res. Appl. 24 (6) (2016) 781–799.

[32] A. Laouadi, A. Parekh, Optical models of complex fenestration systems, Light. Res. Technol. 39 (2) (2007) 123–145.

[33] C. Curcija, S. Vidanovic, R. Hart, J. Jonsson, R. Powles, R. Mitchell, WINDOW Technical Documentation, Lawrence Berkeley National Laboratory Berkeley, California, 2018.

[34] G. Molina, W. Bustamante, J. Rao, P. Fazio, S. Vera, Evaluation of radiance's genBSDF capability to assess solar bidirectional properties of complex fenestration systems, J. Build. Perform. Simulat. 8 (4) (2015) 216–225.

[35] Y. Sun, R. Wilson, H. Liu, Y. Wu, Numerical investigation of a smart window system with thermotropic parallel Slat-Transparent Insulation Material for building energy conservation and daylight autonomy, Build. Environ. (2021) 108048.

[36] EN 673:2011, Glass in Building - Determination of Thermal Transmittance (U Value) - Calculation Method, 2011.

[37] Y. Sun, K. Shanks, H. Baig, W. Zhang, X. Hao, Y. Li, B. He, R. Wilson, H. Liu, S. Sundaram, Integrated semi-transparent cadmium telluride photovoltaic glazing into windows: energy and daylight performance for different architecture designs, Appl. Energy 231 (2018) 972–984.

[38] Lawrence Berkeley National Laboratory, IGDB Database Detailed Installation/ Update Instructions, 2019. Available from: https://windows.lbl.gov/tools/ knowledge-base/articles/igdb-database-detailed-installation-update-instructions.

[39] ISO 9050, Glass in Building-Determination of Light Transmittance, Solar Direct Transmittance, Total Solar Energy Transmittance, Ultraviolet Transmittance and Related Glazing Factors, 2003.

[40] Y. Sun, Y. Wu, R. Wilson, A review of thermal and optical characterisation of complex window systems and their building performance prediction, Appl. Energy 222 (2018) 729–747.

[41] Y. Sun, D. Liu, J.-F. Flor, K. Shank, H. Baig, R. Wilson, H. Liu, S. Sundaram, T. K. Mallick, Y. Wu, Analysis of the daylight performance of window integrated photovoltaics systems, Renew. Energy 145 (2020) 153–163.

[42] A. McNeil, E.S. Lee, J.C. Jonsson, Daylight performance of a microstructured prismatic window film in deep open plan offices, Build. Environ. 113 (2017) 280–297.

[43] Y. Sun, Y. Wu, R. Wilson, Analysis of the daylight performance of a glazing system with parallel Slat transparent insulation material (PS-TIM), Energy Build. 139 (2017) 616–633.

[44] ISO 10077-1:2006, Thermal Performance of Windows, Doors and Shutters-Calculation of Thermal Transmittance -Part 1, General, 2006.

[45] ISO 15099:2003, Thermal Performance of Windows, Doors and Shading Devices -Detailed Calculations, 2003.

[46] National Renewable Energy Laboratory (NREL), EnergyPlus documentation, on-site generation, Available from: https://www.energyplus.net/sites/default/files /docs/site_v8.3.0/EngineeringReference/14-OnSiteGeneration/index.html.

[47] S. Dubey, J.N. Sarvaiya, B. Seshadri, Temperature dependent photovoltaic (PV) efficiency and its effect on PV production in the world-a review, Energy Proc. 33 (2013) 311–321.

[48] O.Z. Sharaf, M.F. Orhan, Concentrated photovoltaic thermal (CPVT) solar collector systems: Part I-Fundamentals, design considerations and current technologies, Renew. Sustain. Energy Rev. 50 (2015) 1500–1565.

[49] Ministry of Housing Communities & Local Government, Approved Document L2A: Conservation of Fuel and Power in New Buildings Other than Dwellings, 2013 Edition with 2016 Amendments, 2016.

[50] Butcher, K.J., CIBSE Guide B - Heating, Ventilating, Air Conditioning and Refrigeration. CIBSE.

[51] I. Korolija, L. Marjanovic-Halburd, Y. Zhang, V.I. Hanby, UK office buildings archetypal model as methodological approach in development of regression models for predicting building energy consumption from heating and cooling demands, Energy Build. 60 (2013) 152–162.

[52] F. Favoino, Y. Cascone, L. Bianco, F. Goia, M. Zinzi, M. Overend, V. Serra, M. Perino, Simulating switchable glazing with energyplus: an empirical validation and calibration of a thermotropic glazing model, in: Proceedings of Building Simulation, 2015.

[53] ASHRAE, ANSI/ASHARE Standard 140-2017 - Standard Method of Test for the Evaluation of Building Energy Analysis Computer Programs, 2017.

[54] H. Tian, W. Zhang, L. Xie, Y. Wu, Y. Sun, M. Chen, W. Wang, X. Wu, Study on the energy saving potential for semi-transparent PV window in Southwest China, Energies 11 (11) (2018) 3239.

[55] S.A. Kalogirou, Solar Energy Engineering: Processes and Systems, Academic Press, 2013.

[56] R. Tällberg, B.P. Jelle, R. Loonen, T. Gao, M. Hamdy, Comparison of the energy saving potential of adaptive and controllable smart windows: a state-of-the-art review and simulation studies of thermochromic, photochromic and electrochromic technologies, Sol. Energy Mater. Sol. Cell. 200 (2019), 109828.